Supporting Information: Influence of North Atlantic climate variability on glacier mass balance in Norway, Sweden, and Svalbard

David Brooking Bonan[1], John Erich Christian[2], Knut Christianson[2]

[1]*Department of Atmospheric Sciences, University of Washington, Seattle, WA, USA*

[2]*Department of Earth and Space Sciences, University of Washington, Seattle, WA, USA*

Correspondence: David Bonan <dbonan@uw.edu>

CONTENTS

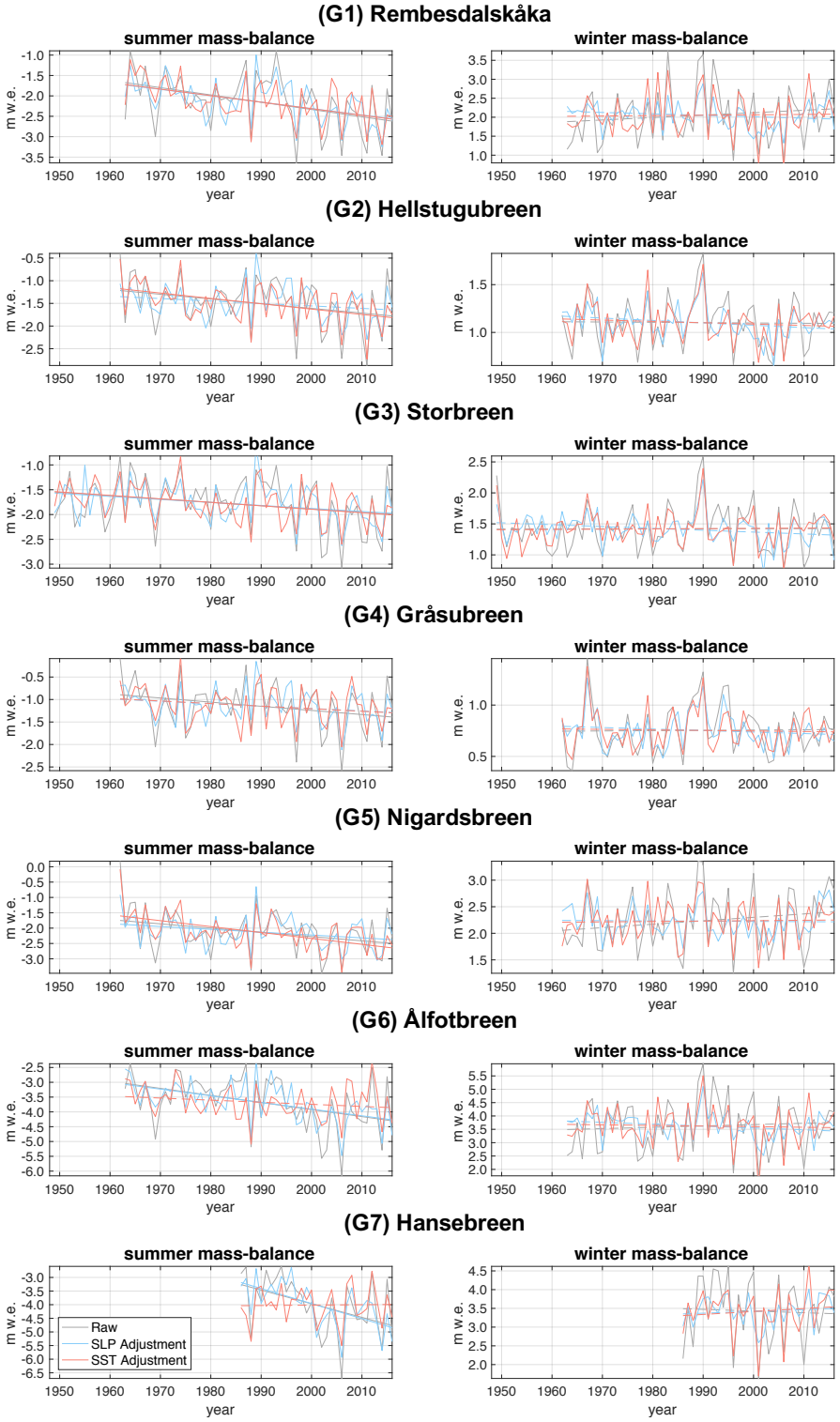

Fig. S1. The raw (gray), adjusted with SLP variability (blue), and adjusted with SST variability (red) summer and winter mass-balance time series for G1-G7. The lines represent a least squares linear fit of each time series. Dashed lines denote insignificant trends and solid lines denote significant trends based on the t-test presented in Section 3.

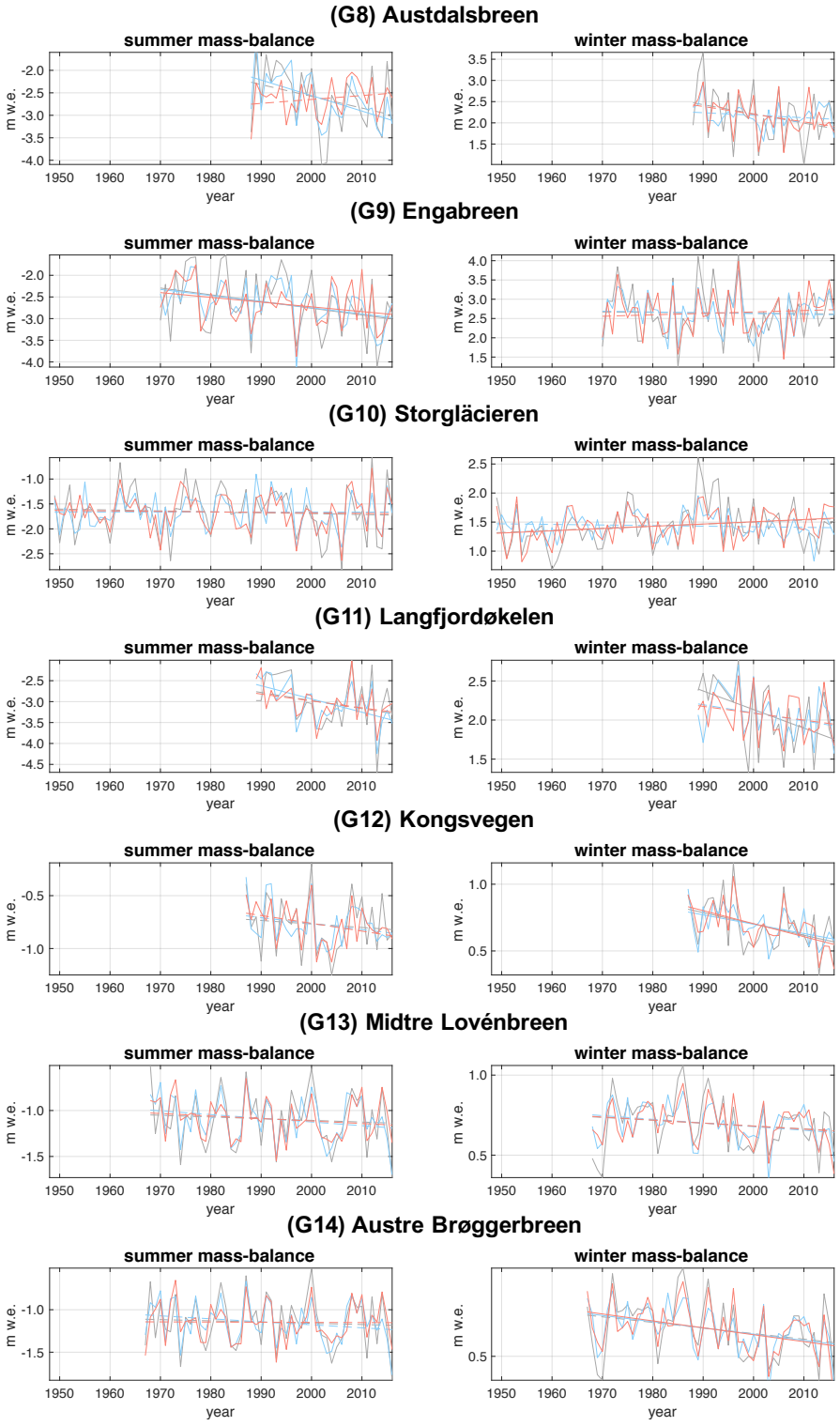

Fig. S2. The raw (gray), adjusted with SLP variability (blue), and adjusted with SST variability (red) summer and winter mass-balance time series for G8-G14. The lines represent a least squares linear fit of each time series. Dashed lines denote insignificant trends and solid lines denote significant trends based on the t-test presented in Section 3.

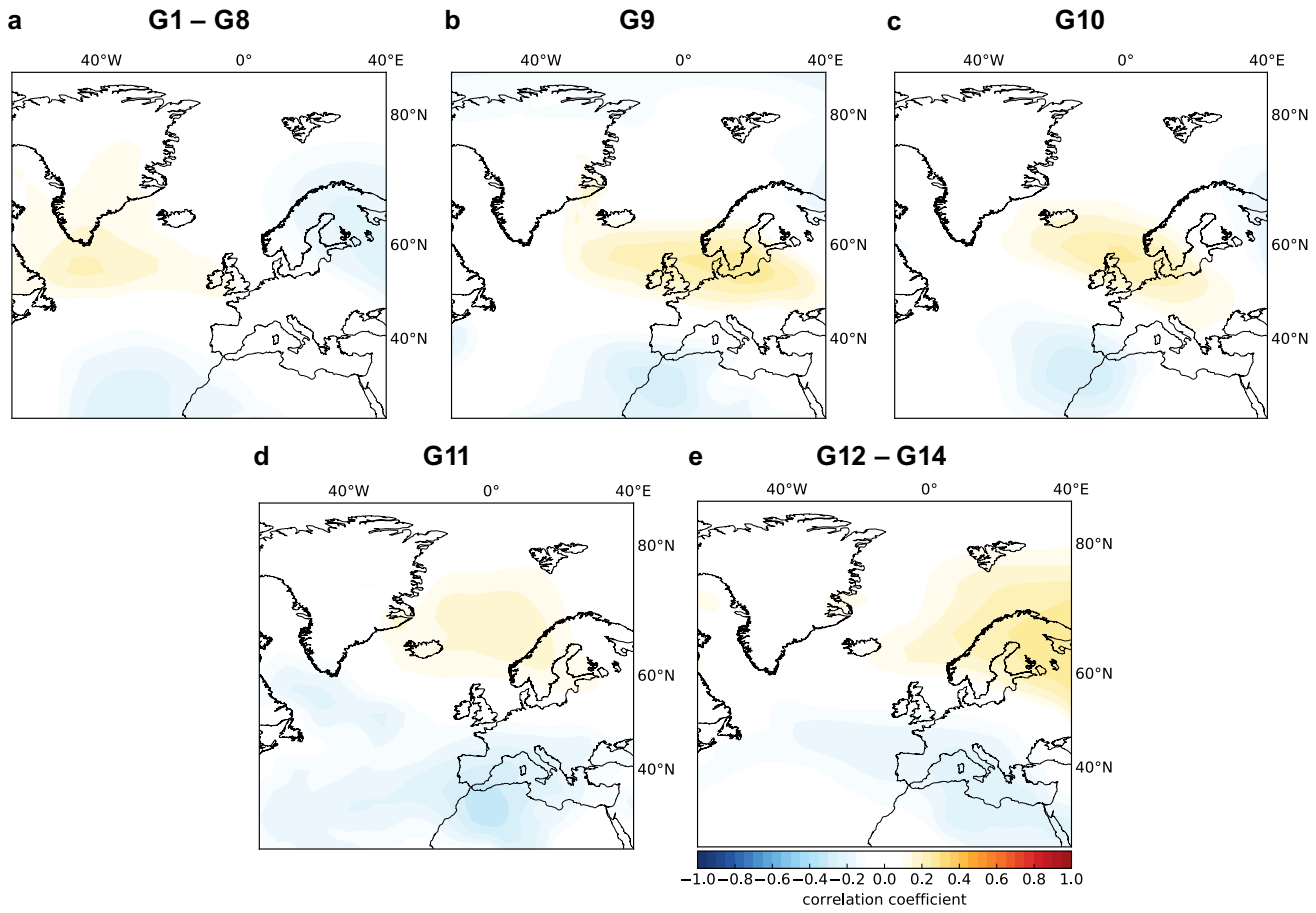

Fig. S3. Predictor patterns for the second mode of wintertime SLP and the winter mass-balance of (a) G1-G8, (b) G9, (c) G10, (d) G11, and (e) G12-G14. The predictor patterns of G1-G8 and G12-G14 are both the average of each individual glacier's predictor pattern.

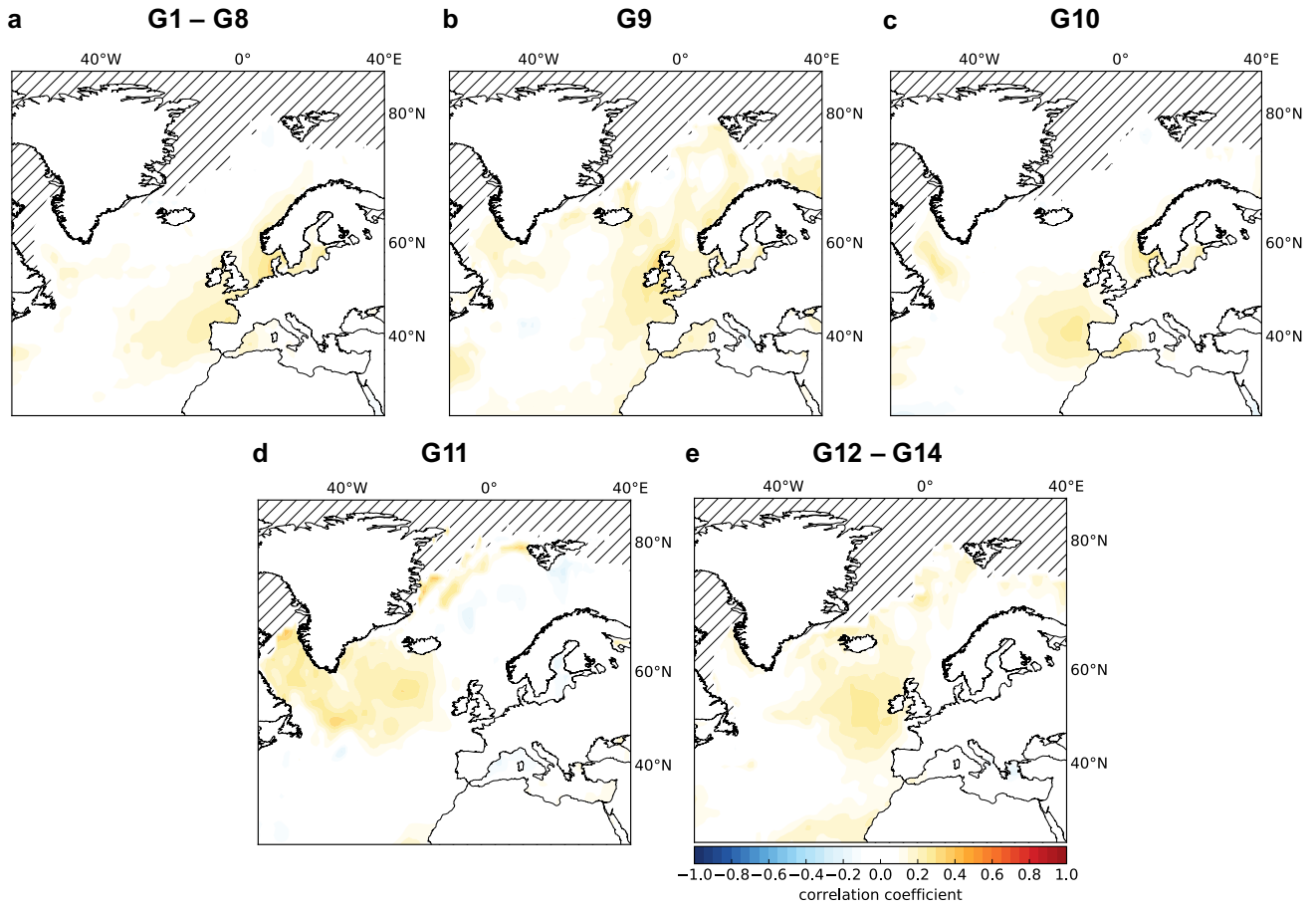

Fig. S4. Predictor patterns for the second mode of wintertime SST and the winter mass-balance of (a) G1-G8, (b) G9, (c) G10, (d) G11, and (e) G12-G14. The patterns shown for G1-G8 and G12-G14 are both the average of each individual glacier's predictor pattern. The gray hatches mark areas removed from the analysis due to the influence of sea ice.

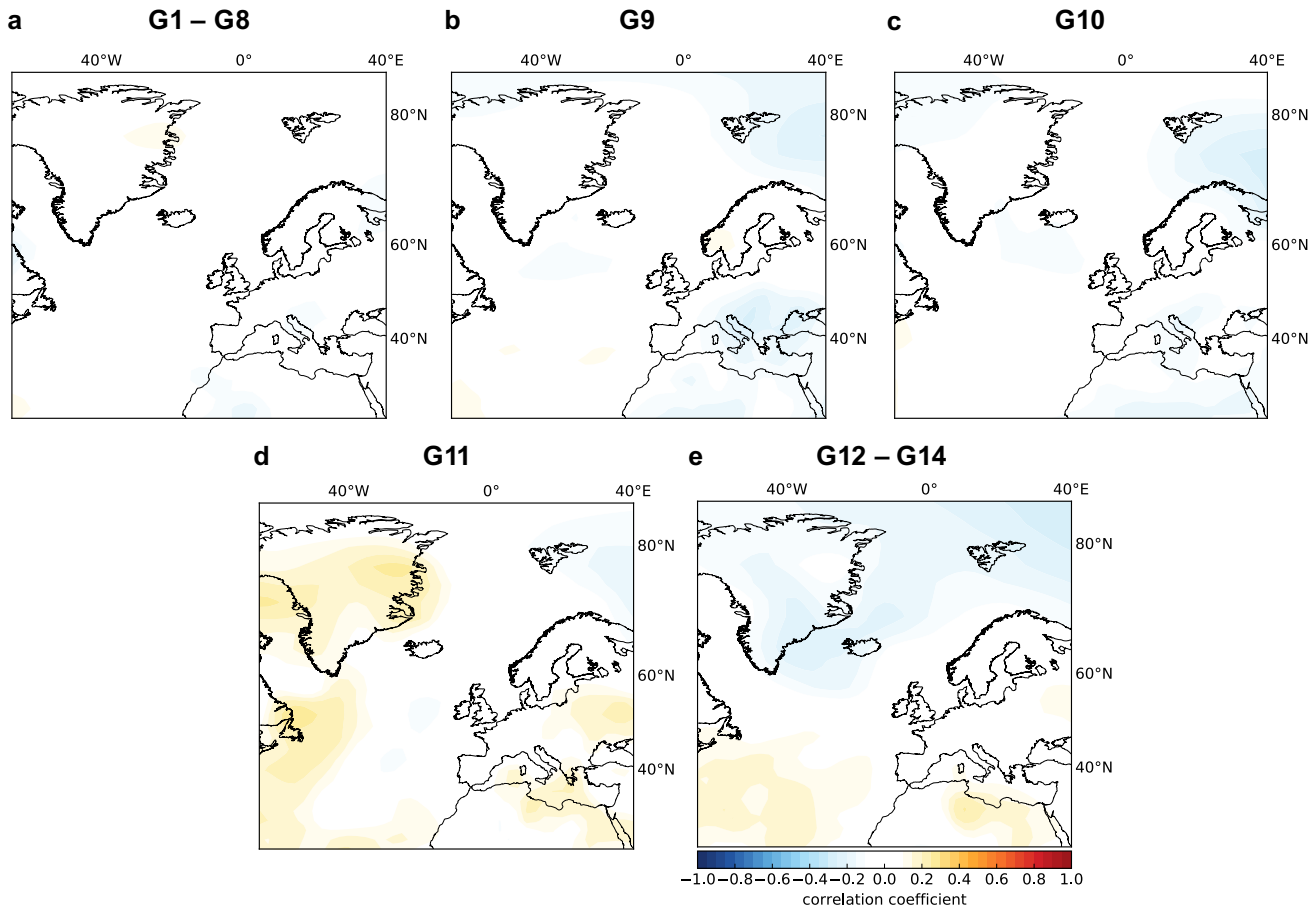

Fig. S5. Predictor patterns for the second mode of summertime SLP and the summer mass-balance of (a) G1-G8, (b) G9, (c) G10, (d) G11, and (e) G12-G14. The patterns shown for G1-G8 and G12-G14 are both the average of each individual glacier's predictor pattern.

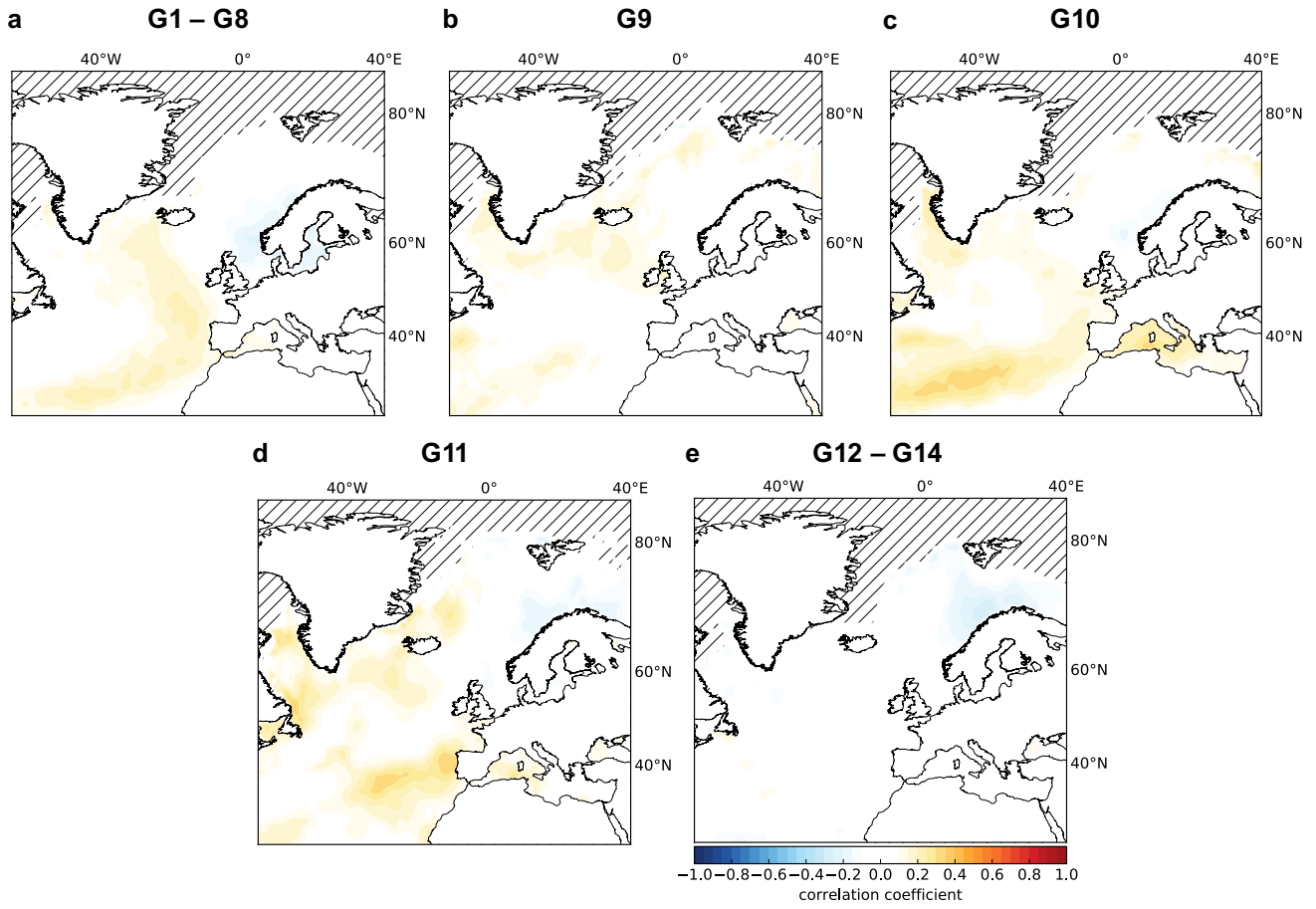

Fig. S6. Predictor patterns for the second mode of summertime SST and the summer mass-balance of (a) G1-G8, (b) G9, (c) G10, (d) G11, and (e) G12-G14. The patterns shown for G1-G8 and G12-G14 are both the average of each individual glacier's predictor pattern. The gray hatches mark areas removed from the analysis due to the influence of sea ice.

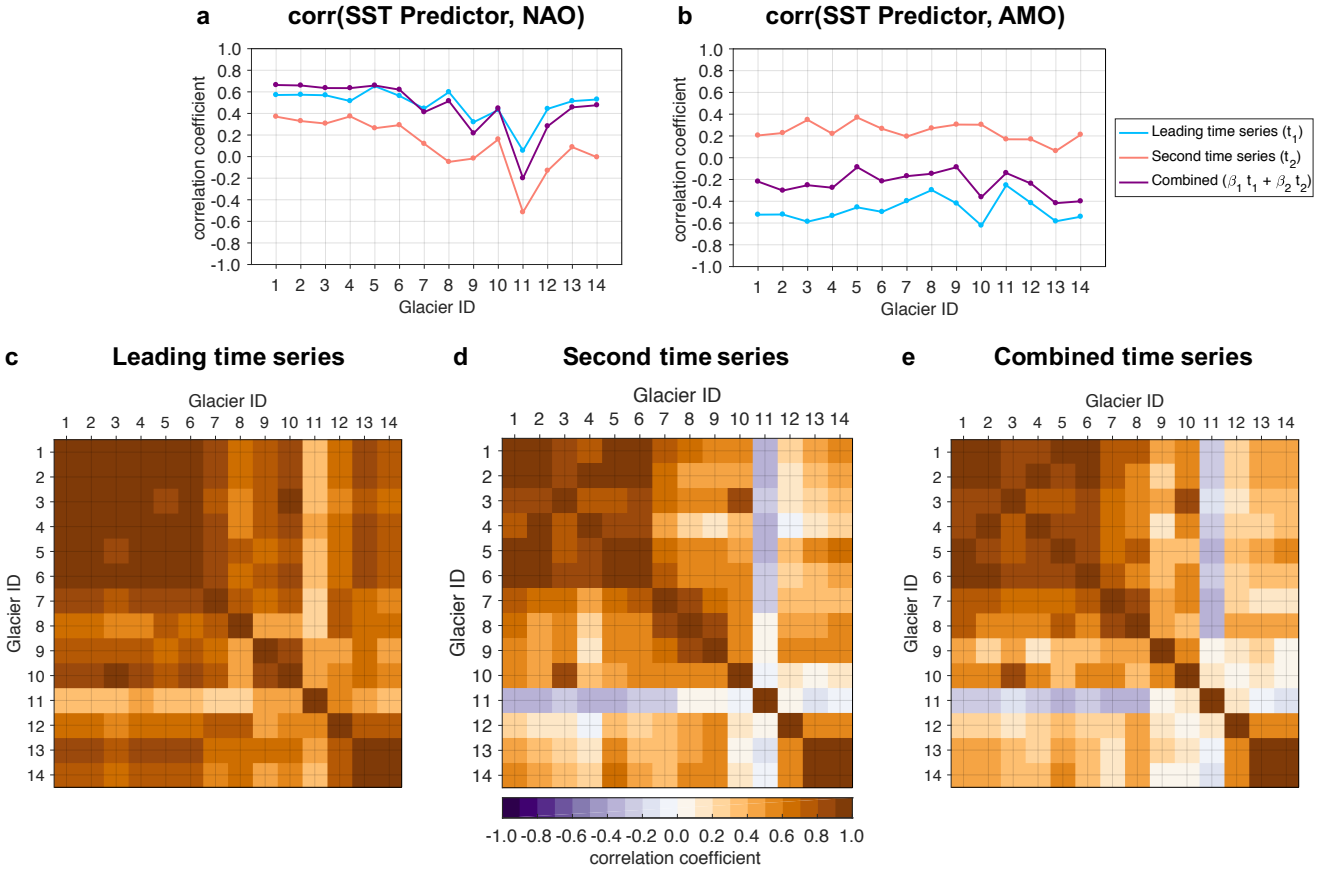

Fig. S7. (a-b) Correlations between climate indices and the SST predictor time series identified by dynamical adjustment each winter mass-balance record. Correlations are shown for the two leading time series alone ($\mathbf{t}_1$ and $\mathbf{t}_2$), and their weighted combinations ($\beta_1\mathbf{t}_1$ and $\beta_2\mathbf{t}_2$). (a) Winter (October-March) NAO index and SST predictors. (b) Winter AMO index and SST predictors. (c-e) Inter-glacier correlations of the leading PLS time series (c), the second time series (d), and the combined time series (e).